Applied Geochemistry 100 (2019) 223–233

Contents lists available at ScienceDirect

Applied Geochemistry

journal homepage: www.elsevier.com/locate/apgeochem

$^{226}Ra/^{238}U$ and $^{228}Th/^{228}Ra$ disequilibrium as weathering indices in beach sand sediments associated with granitoids from Cyclades. Greece

A. Papadopoulos

Department of Mineralogy, Petrology and Economic Geology, School of Geology, Aristotle University of Thessaloniki, 54124, Thessaloniki, Greece

ARTICLE INFO

Keywords:
Secular equilibrium
Weathering indices
Radionuclides
Sediments
Uranium
Thorium

ABSTRACT

Radioactive secular disequilibrium measured as the absolute difference from 1 of the $^{226}Ra/^{238}U$ and $^{228}Ra/^{228}Th$ ratios have been used to determine weathering extent. Twenty-eight samples from beach sands of Cyclades islands, all of them being the weathering products of the local granitic plutons, are studied for their secular disequilibrium in both ^{238}U and ^{232}Th series ($^{226}Ra/^{238}U$ and $^{228}Th/^{228}Ra$ respectively). The results are compared to weathering indices already in use worldwide and suggest a significant linear correlation of U-series disequilibrium with WIP (alkaline and alkaline-earth element leaching) and PWI (silica leaching) for the beach sands studied and significant non-linear correlations with CIA (chemical index of alteration) and PIA (plagioclase index of alteration). Considering only the heavy mineral enriched samples, significant correlations exist between U-series disequilibrium and CIA, CIW (chemical index of weathering) and PIA. Therefore, with an appropriate choice of the weathering index and samples both U-series and weathering index can recover the extent of chemical weathering. On the other hand, the use of Th-series disequilibrium as a weathering index is limited, due to ^{228}Th and ^{228}Ra geochemistry and especially due to their short radionuclide half-lives. U-series disequilibrium can therefore be used as a relatively sensitive weathering index in sediments consistent with CIA, CIW and PIA indices. However, the mineralogical composition must be considered. More specifically the mineral content of the sediments should involve considerable amounts of sensitive to weathering minerals (e.g. Fe-Mg minerals) as well as feldspars.

1. Introduction and objectives

The natural radionuclides ^{238}U, ^{235}U, and ^{232}Th and their decay products have different chemical and physical properties and half-lives ranging from < 1 s up to thousands of millions years. The study of the ratios of ^{238}U-series and ^{232}Th-series radionuclides in plutonic rocks, allows the study of post-magmatic processes and more specifically, rock–water interactions with implications about the suitability for nuclear waste disposal, the determination of the age of deposits younger than 1 Ma, mantle evolution, hydrological tracing and the determination of mineral weathering rates (Bonotto et al., 2001; Chapman and Smellie, 1986; Condomines et al., 1988; Gascoyne and Schwarcz, 1986; Gascoyne and Schwarcz, 1986, 1986; Guthrie, 1991; Guttman and Kronfeld, 1982; Schwarcz et al., 1982; Smellie, 1982; Smellie et al., 1986; Schwarcz and Gascoyne, 1984; Rihs et al., 2013).

In an undisturbed isotopic system, the activity of the parent radionuclide is similar to that of its intermediate or final decay product. Therefore the decay rates of the radionuclides of a particular isotopic system is nearly the same. This state of a radioactive series is defined as permanent radioactive equilibrium (radioactive secular equilibrium).

The isotopic system can be disturbed when the parent radionuclide or its decay products enter or depart from the isotopic system, during a period comparable to the half-life period of the daughter radionuclide. In that case there is a radioactive secular disequilibrium (Rosholt, 1983; Smellie et al., 1986; Gascoyne and Cramer, 1987; Latham and Schwarcz, 1987).

The causes of the disturbance of radioactive secular equilibrium are usually related to geochemical processes that cause the mobilisation of a radionuclide during a period comparable to the half-life period of the daughter radionuclide (Osmond and Cowart, 1982). These geochemical mechanisms concern the dissolution and migration of more geochemically soluble radionuclides of a radioactive series, the diffusion of nuclides of radon and the effects of α-particle recoil (Gascoyne, 1992; Ivanovich and Harmon, 1982, 1992; Osmond and Cowart, 1976, 1982).

In order to investigate the presence of radioactive secular equilibrium in an isotopic system, the activity of the long half-life parent radionuclide is correlated to one of its decay products having significantly shorter half-life (Osmond et al., 1983). The state of radioactive secular disequilibrium however, is a non-steady state and the time needed for the radioactive equilibrium to be restored depends on

E-mail address: argpapad@geo.auth.gr.

https://doi.org/10.1016/j.apgeochem.2018.12.002
Received 16 January 2018; Received in revised form 13 November 2018; Accepted 1 December 2018
Available online 04 December 2018
0883-2927/ © 2018 Elsevier Ltd. All rights reserved.

Table 1
Description of the weathering indices used for comparisons.

Index	Formula	Value for unweathered samples	Values of maximum weathering
R	SiO_2/Al_2O_3	10	0
WIP	$100*[(2Na_2O/0.35)+(MgO/0.9)+(2K_2O/0.25)+(CaO/0.7)]$	> 100	0
PWI	$100*[SiO_2/(TiO_2 + Fe_2O_3 + SiO_2 + Al_2O_3)]$	> 50	0
V	$(Al_2O_3 + K_2O)/(MgO + CaO + Na_2O)$	> 1	Infinite
CIA	$100*[(Al_2O_3/Al_2O_3 + CaO + Na_2O + K_2O)]$	≤ 50	100
CIW	$100*[(Al_2O_3/Al_2O_3 + CaO + Na_2O)]$	≤ 50	100
PIA	$100*[(Al_2O_3–K_2O/Al_2O_3 + CaO + Na_2O–K_2O)]$	≤ 50	100

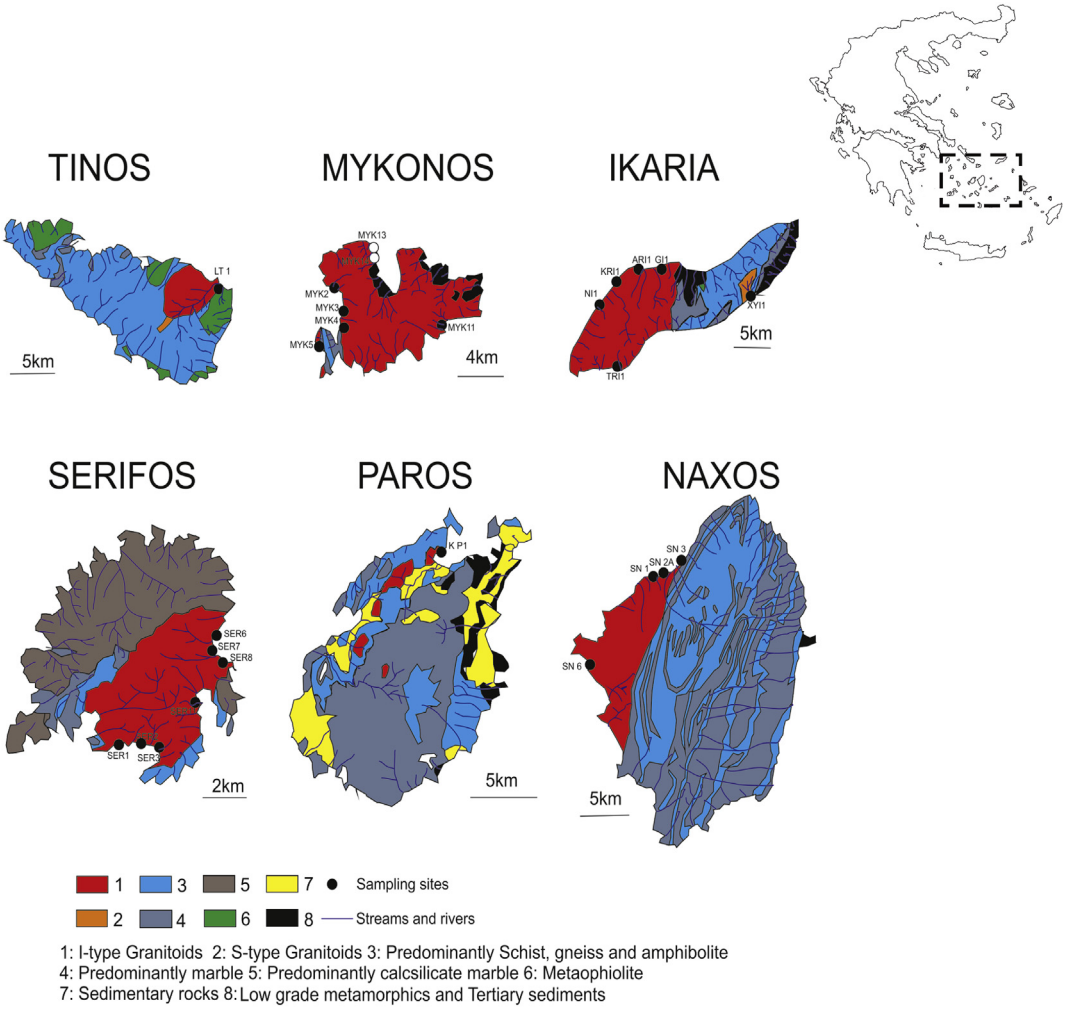

Fig. 1. Geological map of the plutonic rocks of the Atticocycladic zone including the sampling sites.

the decay rate of the radionuclides. In the case of ^{238}U radioactive series, the equilibrium between the parent–daughter radionuclide will be restored at a period equal to five or six times the half-life of the daughter radionuclide (Dosseto et al., 2008).

Plutonic rocks can usually be considered to be in radioactive secular equilibrium due to their crystallisation age which is usually above 5 Ma. However, in case the rock is fractured or/thus chemically altered, the isotopic system can be affected by the interaction between the rock and the groundwater. All the above can cause the mobilisation of the U isotopes (^{238}U, ^{234}U) and ^{226}Ra which under oxidising conditions are significantly more mobile than ^{230}Th. The latter is geochemically immobile and cannot be removed easily under the pH conditions expected during weathering (circumneutral) (Gascoyne and Schwarcz, 1986). There is also a possibility for its isotopic system to be out of secular equilibrium due to the presence of a-particle recoil.

Weathering indices are useful in surface geology studies. Some of them are explained below and given in Table 1:

Ruxton Ratio (R): This index is best fitted to samples with felsic to intermediate parental rocks and was introduced by Ruxton (1968). Taking into account that alumina is immobile, it relates silica loss to total element.

Weathering Index of Parker (WIP). This index introduced by Parker (1970) for felsic, intermediate and mafic rocks, is based on the proportions of alkaline and alkaline-earth metals (sodium, potassium, magnesium and calcium) present which are the most mobile major elements during weathering. WIP also takes into account the individual mobility of sodium, potassium, magnesium and calcium, based on their bond strengths with oxygen (Parker, 1970).

Product of Weathering Index (PWI): This index can be used to identify the initial and lateral products of weathering which can be

Table 2
Location, neighbouring granitic samples and textural characteristics of the samples studied.

Sample	Granitic samples	Comments	Sample type	Textural group	Sediment name
	Close to the sampling sites of beach sands				
Naxos					
SN1	AAN1, APN1, VN1		Bimodal. Moderately Sorted	Slightly Gravelly Sand	Slightly Very Fine Gravelly Fine Sand
SN2A		Heavy minerals horizon	Bimodal. Moderately Sorted	Slightly Gravelly Sand	Slightly Very Fine Gravelly Fine Sand
SN3		Heavy minerals horizon	Unimodal. Well Sorted	Slightly Gravelly Sand	Slightly Medium Gravelly Fine Sand
SN6		Heavy minerals horizon	Unimodal. Poorly Sorted	Slightly Gravelly Sand	Slightly Very Fine Gravelly Fine Sand
Serifos					
SER1	KAS1, XS1		Trimodal. Poorly Sorted	Gravelly Sand	Medium Gravelly Coarse Sand
SER2		Heavy minerals horizon	Polymodal. Poorly Sorted	Gravelly Sand	Medium Gravelly Fine Sand
SER3		Heavy minerals horizon	Bimodal. Moderately Sorted	Slightly Gravelly Sand	Slightly Very Fine Gravelly Fine Sand
SER6			Unimodal. Well Sorted	Slightly Gravelly Sand	Slightly Fine Gravelly Fine Sand
SER7			Unimodal. Very Well Sorted	Sand	Very Well Sorted Fine Sand
SER8			Trimodal. Very Poorly Sorted	Gravelly Sand	Medium Gravelly Fine Sand
SER11			Trimodal. Poorly Sorted	Slightly Gravelly Sand	Slightly Very Fine Gravelly Coarse Sand
Paros					
KP1	NP1, KP2		Bimodal. Moderately Sorted	Slightly Gravelly Sand	Slightly Medium Gravelly Fine Sand
Tinos					
LT1	T12C, T31B, T34, T45A	Heavy minerals horizon	Unimodal. Very Well Sorted	Slightly Gravelly Sand	Slightly Very Fine Gravelly Fine Sand
Mykonos					
MYK3	TUM1, PLM1		Polymodal. Poorly Sorted	Sandy Gravel	Sandy Very Fine Gravel
MYK4			Polymodal. Poorly Sorted	Gravelly Sand	Very Fine Gravelly Fine Sand
MYK5			Bimodal. Poorly Sorted	Slightly Gravelly Sand	Slightly Very Fine Gravelly Fine Sand
MYK2			Trimodal. Poorly Sorted	Slightly Gravelly Sand	Slightly Very Fine Gravelly Fine Sand
MYK17			Trimodal. Poorly Sorted	Gravelly Sand	Very Fine Gravelly Coarse Sand
MYK15			Polymodal. Poorly Sorted	Gravelly Sand	Very Fine Gravelly Very Coarse Sand
MYK11			Polymodal. Poorly Sorted	Gravelly Sand	Very Fine Gravelly Coarse Sand
MYK13			Bimodal. Poorly Sorted	Slightly Gravelly Sand	Slightly Medium Gravelly Fine Sand
MYK14		Heavy minerals horizon	Unimodal. Moderately Well Sorted	Slightly Gravelly Sand	Slightly Very Fine Gravelly Fine Sand
Ikaria					
ARI1	AI2, API2, KI2		Trimodal. Poorly Sorted	Slightly Gravelly Sand	Slightly Very Fine Gravelly Coarse Sand
TRI1			Bimodal. Moderately Sorted	Slightly Gravelly Sand	Slightly Very Fine Gravelly Coarse Sand
GI1			Trimodal. Moderately Well Sorted	Slightly Gravelly Sand	Slightly Very Fine Gravelly Coarse Sand
NI1			Polymodal. Poorly Sorted	Gravelly Sand	Very Fine Gravelly Coarse Sand
KRI1			Polymodal. Poorly Sorted	Gravelly Sand	Very Fine Gravelly Coarse Sand
XYI1			Polymodal. Poorly Sorted	Sandy Gravel	Sandy Very Fine Gravel

tracked at the same time and is proper to track movements of less mobile elements (Souri et al., 2006).

Vogt's Residual Index (V): It was first introduced by Vogt in 1927. Considering the bulk chemistry of moraine and marine clay deposits, this index was used to determine the weathering status of clays in Quaternary deposits of the Numedal Area in Norway (Roaldset, 1972).

Chemical Index of Alteration (CIA): It was firstly proposed by Nesbitt and Young (1982). CIA gives the extent of feldspars alteration to clays (Fedo et al., 1995; Maynard et al., 1995; Nesbitt and Young, 1984, 1989).

Chemical Index of Weathering (CIW): CIW index was introduced by Harnois and Moore (1988). It is identical to CIA. However, CIW does not consider K_2O. CIW is also a measure of the extent of feldspars alteration to clays (Fedo et al., 1995; Maynard et al., 1995; Nesbitt and Young, 1984, 1989).

Plagioclase Index of Alteration (PIA): PIA may be used when plagioclase weathering needs to be monitored (Fedo et al., 1995).

Plutonic rocks and more specifically granitic rocks can be considered as closed isotopic systems. Atticocycladic zone, located in Greece, central Aegean Sea, is mainly comprised by pre-Alpidic basement and is intruded by numerous plutonic rocks. Given the fact that the majority of the granitic rocks of Atticocycladic zone are in radioactive secular equilibrium (Papadopoulos et al., 2013) and considering that the granitic rocks of the Atticocycladic zone are the most probable parental rocks of the beach sand samples studied (Papadopoulos et al., 2016a; Papadopoulos, 2018), this work aims to compare the results of some of the weathering indices in use with the results of radioactive secular disequilibrium between ^{226}Ra and ^{238}U as well as between ^{228}Th and ^{228}Ra in the beach sands. Similar comparisons have already been made for the beach sands from Kavala and Sithonia (N. Greece) by (Papadopoulos et al., 2016b), showing that radioactive disequilibrium in ^{238}U-series can be used as weathering index. Therefore, assuming that their parental rocks are in secular equilibrium (Papadopoulos et al., 2013), any distortions in the ^{226}Ra-^{238}U or ^{228}Th-^{228}Ra systems of the beach sands have occurred during their weathering and transport. So, these radionuclide ratios proposed could be used as weathering indices in some cases. Of course, we must note that measuring isotopic ratios can be much more tricky than measuring major elements. However, these particular isotopic ratios can be used as relatively sensitive weathering indices, especially when minerals susceptible to weathering are present (micas, amphiboles, epidote, allanite etc.).

2. Materials and methods

2.1. Geological setting

The Atticocycladic zone is comprised mainly of two tectonic units (Durr et al., 1978). The lower unit is formed of a pre-Alpidic basement (gneisses, schists and marbles), Mesozoic marbles, meta-volcanics and meta-pelites. The upper unit consists of ophiolitic rocks, Permian

Fig. 2. Sampling sites.

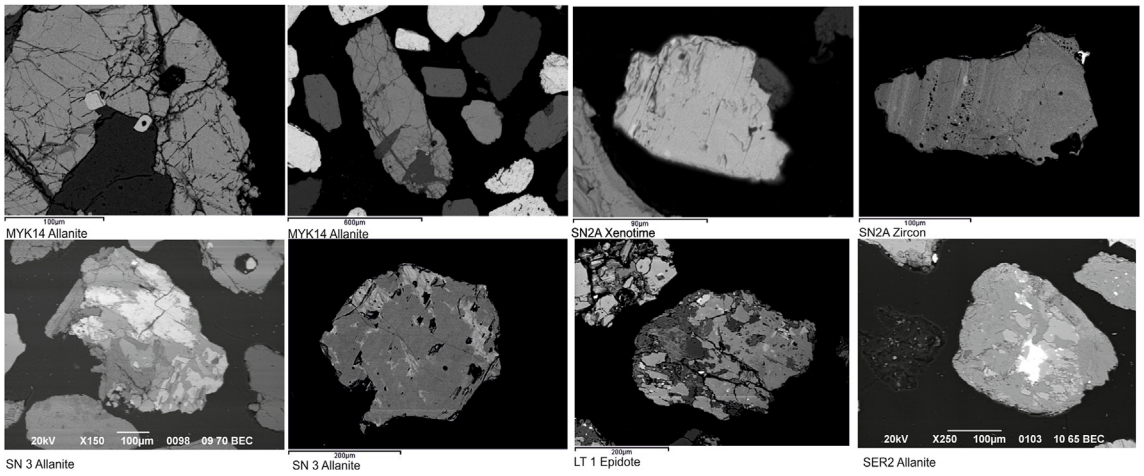

Fig. 3. Back scattered electron images of selected grains of separated heavy minerals.

sediments and high-temperature metamorphic rocks. Evidence of a poly-metamorphic history suggest a high-pressure, blueschist facies metamorphism dated at middle Eocene, a medium-pressure metamorphism at around the Oligocene-Miocene, followed by the intrusion of granitic magmas. They can be distinguished into: (a) I-type granites, granodiorites and dykes with similar composition and (b) peraluminous two-mica granites and leucogranites with S-type characteristics (Pe-Piper and Piper, 2002 and references therein).

The granitic intrusions are placed in Serifos, Mykonos, Tinos, Paros, Naxos, Delos, Rinia and Ikaria islands. The petrography, geochemistry, petrogenesis and age of the granites of this zone have been extensively studied by various researchers (Altherr et al., 1982, 1988; Buick, 1991; Pe-Piper et al., 1997, 2002; Pe-Piper, 2000; Altherr and Siebel, 2002; Pe-Piper and Piper, 2002; Mastrakas, 2006; Skarpelis et al., 2008; Iglseder et al., 2009; Stouraiti et al., 2010).

More specifically, Paros pluton (Miocene; Altherr et al., 1982) consists of S-type fine to medium grained two-mica granite. It is located mainly to the NW of the Paros island.

In Naxos island, two plutonic bodies are present, one at the western part of the island and one at the central northern part. The western plutonic body is a mid-to coarse-grained biotite granodiorite (Pe-Piper et al., 1997) consisting of quartz, feldspars, biotite, hornblende, zircon, apatite, titanite, magnetite and ilmenite, and is considered as an I-type intrusion of Miocene age intruding the metamorphic basement of the Atticocycladic zone (Pe-Piper et al., 1997). The central northern plutonic body consists mainly of an S-type two-mica granite (Altherr et al., 1982) of Miocene age (Pe-Piper et al., 1997).

Mykonos pluton covers the largest part of the island of Mykonos and its main rock-type is biotite granodiorite (Pe-Piper et al., 2002). It is considered as an I-type intrusion of Miocene age (Henjes-Kunst et al., 1988). Low-temperature hydrothermal fluids activity resulted locally in the chloritisation of Fe-Mg minerals. Mineral precipitation is present in the NW and NE part of the island. It occurs as barite and Fe-hydroxide impregnations in the late Miocene sedimentary unit and as silicified

Table 3
Activities of ^{238}U, ^{226}Ra, ^{228}Ra and ^{228}Th ($Bq \cdot kg^{-1}$), $^{226}Ra/^{238}U$, $^{228}Ra/^{228}Th$, along with the respective standard errors (± σ) and absolute differences from 1.

	^{238}U- series				^{232}Th- series					± σ		± σ	1-[$^{226}Ra/^{238}U$]	1-[$^{228}Ra/^{228}Th$]
	^{238}U	± σ	^{226}Ra	± σ	^{228}Ra	± σ	^{228}Th	± σ	$^{226}Ra/^{238}U$		$^{228}Ra/^{228}Th$			
Naxos														
SN1	15	5	14	1	18	1	17	1	0.93	0.02	0.94	0.04	0.07	0.06
SN2A	233	9	206	3	619	14	616	10	0.88	0.02	1.00	0.04	0.12	0.00
SN3	53	5	56	1	111	3	110	2	1.06	0.02	0.99	0.04	0.06	0.01
SN6	495	17	446	5	1634	32	1664	22	0.90	0.02	1.02	0.04	0.10	0.02
Serifos														
SER1	44	5	46	1	30	1	30	1	1.05	0.02	1.00	0.04	0.05	0.00
SER2	21	5	26	1	25	1	26	1	1.24	0.02	1.04	0.04	0.24	0.04
SER3	29	3	36	1	20	1	20	1	1.24	0.02	1.00	0.04	0.24	0.00
SER6	107	4	110	1	120	3	118	1	1.03	0.02	0.98	0.06	0.03	0.02
SER7	44	4	41	1	61	2	63	1	0.93	0.02	1.03	0.05	0.07	0.03
SER8	21	4	22	1	23	1	24	1	1.05	0.02	1.04	0.04	0.05	0.04
SER11	90	7	81	1	29	1	31	1	0.90	0.01	1.07	0.04	0.10	0.07
Paros														
KP1	56	6	50	1	62	1	59	1	0.89	0.01	0.95	0.04	0.11	0.05
Tinos														
LT1	19	5	12	1	19	1	14	1	0.63	0.02	0.74	0.04	0.37	0.26
Mykonos														
MYK3	96	6	78	1	271	5	275	2	0.81	0.01	1.01	0.06	0.19	0.01
MYK4	26	6	25	1	39	2	40	1	0.96	0.01	1.03	0.05	0.04	0.03
MYK5	119	9	82	1	520	9	527	3	0.69	0.01	1.01	0.06	0.31	0.01
MYK2	66	7	55	1	182	4	180	2	0.83	0.01	0.99	0.05	0.17	0.01
MYK17	56	6	53	1	62	2	63	1	0.95	0.01	1.02	0.05	0.05	0.02
MYK15	21	5	26	1	27	1	27	1	1.24	0.02	1.00	0.04	0.24	0.00
MYK11	73	7	58	1	185	3	185	1	0.79	0.01	1.00	0.06	0.21	0.00
MYK13	63	5	58	1	215	5	216	2	0.92	0.02	1.00	0.06	0.08	0.00
MYK14	628	30	2292	15	10143	162	9953	47	3.65	0.03	0.98	0.07	2.65	0.02
Ikaria														
ARI1	40	5	28	1	53	2	49	1	0.70	0.02	0.92	0.05	0.30	0.08
TRI1	21	1	27	1	23	1	25	1	1.29	0.04	1.09	0.04	0.29	0.09
GI1	33	4	27	1	21	1	21	1	0.82	0.02	1.00	0.04	0.18	0.00
NI1	47	6	33	1	108	3	110	2	0.70	0.01	1.02	0.04	0.30	0.02
KRI1	34	4	29	1	56	2	57	1	0.85	0.02	1.02	0.05	0.15	0.02
XYI1	21	4	19	1	16	1	17	1	0.90	0.02	1.06	0.04	0.10	0.06

breccia along the main fault zone of the Mykonos brittle detachment. However, the main expression of this mineralization consists of banded barite and/or Fe-hydroxide veins (Menant et al., 2013).

The granitic pluton in Tinos island is located at the SE part of the island intruding ophiolites, gneisses, schists and marbles of the basement. The main rock-type is a medium-grained biotite granodiorite, while a leucogranite is also present at the central part of the island. The first is considered as an I-type intrusion, while the latter as an S-type (Altherr et al., 1982; Altherr et al., 1988). According to Altherr et al. (1982) and Henjes-Kunst et al. (1988). Tinos pluton is of Miocene age. Mastrakas (2006) reported the presence of contact metamorphism and associated skarn mineralization at the NW and SW parts of the pluton.

Serifos pluton is present at the SE part of the island. The main rock-type present is hornblende biotite granodiorite. Contact metamorphism of high temperature and mineralization are associated with the pluton intrusion (Iglseder et al., 2009 and references therein). According to Henjes-Kunst et al. (1988) the pluton is of Miocene age and is considered as an I-type intrusion. Iglseder et al. (2009) considered the leucogranite as an S-type intrusion. The latter is strongly deformed and tectonised.

Two granitic plutons of Miocene age (Altherr et al., 1982) are present in Ikaria Island. One, considered as an I-type intrusion covers most of the western part of the island, and a smaller one at the SE part with characteristics of S-type intrusion (Altherr et al., 1982). The main rock-type of the I-type intrusion is biotite granite. The S-type intrusion is represented by a mid-grained two-mica granite.

2.2. Sampling and pre-treatment of sediments

Twenty-eight representative sediment (sand) samples (separated from each other by around 500 m) were collected from beaches close to the plutonic rocks of the Atticocycladic zone (Fig. 1 and Table 2). Four samples were obtained from Naxos, seven from Serifos, one from Paros, one from Tinos, nine from Mykonos and six from Ikaria island (Fig. 1).

Several samples (MYK14, SN2A, SN3, SN6, LT3, SER2, SER3) were collected from specific horizons of black colour of 1–4 cm, heavily enriched in heavy minerals (Table 2, Fig. 2).

Each sand sample was a result of mixing of three sub-samples of equal mass (~500 g) that were obtained from a depth of 20 cm and were approximately 1.4 m apart, forming an equilateral triangle covering an area of approximately 1 m^2. The three sub-samples were homogenized by mixing in-situ and this sand mixture, weighing approximately 1.5 kg, was considered as representative.

In the laboratory, the samples were cleaned with warm water and dried. Sea shells, etc. were removed by hand picking. To obtain the grain-size distribution of the samples, the 8, 4, 2, 1, 0.5, 0.125 and 0.063 mm ASTM sieves were used. For the mineral separations, the 0.125–0.5 mm grain-size fraction was used, after the determination of the average grain size of the heavy minerals under the binocular microscope. After magnetite removal using a hand magnet, heavy liquid (tetrabromoethane. 2.967 g/cm^3) and a Frantz isodynamic separator were employed to determine the wt.% heavy (HF), the heavy magnetic (HM) and the heavy non-magnetic (HNM) fractions of the whole sample. The HM fraction (< 0.8 amp at forward and side slope of 15° and 25° respectively) contains allanite, amphibole, mica, clinopyroxene, magnetite and hematite while the HNM fraction (> 0.8 amp at same settings) contains zircon, titanite and apatite. All of them were identified under the binocular microscope. Sample preparation and mineral separations were performed at the laboratories of the Department of Mineralogy-Petrology-Economic Geology, School of

Table 4
Major element analyses of the beach sands studied.

Det. Lim.	SiO_2	Al_2O_3	Fe_2O_3	MnO	MgO	CaO	Na_2O	K_2O	TiO_2	P_2O_5	LOI	Total
	%											
	0.01	0.01	0.01	0.00	0.01	0.01	0.01	0.01	0.00	0.01		
SN1	83.25	6.65	1.23	0.025	0.58	2.83	1.22	2.17	0.105	0.02	2.77	100.8
SN2A	58.63	17.13	9.86	0.640	2.27	4.95	0.65	0.99	1.005	0.16	2.25	98.55
SN3	54.97	9.42	11.20	1.049	4.51	8.64	0.73	0.74	1.461	0.10	7.26	100.1
SN6	64.96	11.24	4.32	0.250	1.12	6.93	2.00	2.90	1.832	0.06	3.69	99.29
SER1	53.46	8.74	17.73	0.203	1.56	12.82	1.74	1.20	0.231	0.04	3.15	100.9
SER2	52.28	8.41	20.56	0.210	1.32	8.74	2.12	1.43	0.221	0.05	5.07	100.4
SER3	52.42	10.06	16.09	0.113	0.91	14.98	1.31	0.93	0.835	0.04	1.88	99.55
SER6	83.04	7.43	2.70	0.022	0.18	1.31	1.67	2.22	0.546	0.04	0.64	99.80
SER7	80.61	9.13	1.07	0.012	0.23	2.00	2.30	3.03	0.282	0.02	1.26	99.94
SER8	59.88	9.75	10.18	0.138	0.64	10.80	2.03	2.62	0.503	0.06	2.13	98.72
SER11	73.21	12.10	1.69	0.013	0.40	2.73	2.82	3.53	0.297	0.06	3.06	99.91
KP1	71.71	9.31	1.12	0.026	1.17	6.10	2.28	3.26	0.118	0.04	5.73	100.9
LT1	72.44	10.22	3.94	0.076	2.74	4.15	2.34	1.60	0.407	0.05	1.76	99.71
MYK4	71.60	13.13	1.46	0.022	0.47	4.57	2.61	3.65	0.189	0.05	2.97	100.7
MYK5	67.98	12.69	1.41	0.041	0.41	6.59	2.81	2.57	0.724	0.08	3.41	98.70
MYK2	74.56	11.74	1.15	0.022	0.30	3.00	2.46	3.88	0.286	0.06	1.94	99.39
MYK17	70.59	10.20	4.51	0.240	0.39	1.46	1.88	4.19	0.253	0.06	3.23	97.00
MYK15	80.61	9.62	1.09	0.029	0.19	1.46	1.49	4.74	0.086	0.02	1.45	100.8
MYK11	70.95	13.98	1.33	0.026	0.33	3.19	2.85	4.84	0.370	0.05	1.70	99.61
MYK14	26.12	5.09	13.07	0.272	0.67	5.10	0.71	1.08	8.783	0.06	2.58	63.54
ARI1	85.06	7.57	0.63	0.009	0.13	0.46	1.26	3.77	0.069	0.01	0.75	99.73
TRI1	84.91	8.08	0.95	0.013	0.12	0.62	1.66	3.34	0.072	0.04	0.81	100.6
GI1	87.46	6.01	0.60	0.008	0.08	0.30	0.89	3.37	0.042	< 0.01	0.64	99.42
NI1	78.89	9.93	1.28	0.020	0.38	1.05	1.90	3.90	0.189	0.04	1.40	98.98
KRI1	82.66	9.35	0.95	0.014	0.24	0.63	1.61	3.95	0.187	0.04	1.04	100.7
MYK3	72.36	12.79	1.31	0.023	0.35	3.93	2.70	4.04	0.557	0.05	2.16	100.3
MYK13	77.44	8.28	2.36	0.049	0.41	1.83	1.43	3.86	0.456	0.04	2.57	98.73
XYI1	81.67	7.46	1.72	0.030	0.55	1.78	1.87	1.70	0.260	0.07	1.75	98.85

Table 5
Semi-quantitative mineralogical composition (% wt.) of the heavy magnetic and heavy non-magnetic fractions of selected samples.

	SN2A	SN2A	SER3	SER2	SN3	SN3	LT1	MYK14	MYK14	SN6
	HM	HNM	HM	HM	HM	HNM	HM	HM	HNM	HM
Garnet	53.2	n.d.	47.2	30.5	66.8	n.d.	n.d.	n.d.	n.d.	29.2
Epidote	14.4	n.d.	46.8	28.7	n.d.	n.d.	66.0	n.d.	n.d.	n.d.
Pyroxenes	18.6	n.d.	4.2	24.1	24.1	n.d.	3.4	n.d.	n.d.	43.1
Allanite	n.d.	n.d.	n.d.	n.d.	n.d.	n.d.	n.d.	42.0	n.d.	21.1
Kyanite	n.d.	84.2	n.d.	n.d.	n.d.	n.d.	n.d.	n.d.	n.d.	n.d.
Amphiboles	5.6	n.d.	n.d.	n.d.	5.4	n.d.	30.6	n.d.	n.d.	6.5
Silimanite	n.d.	n.d.	n.d.	n.d.	n.d.	58.3	n.d.	n.d.	n.d.	n.d.
Muscovite	n.d.	8.1	n.d.	n.d.	n.d.	n.d.	n.d.	n.d.	n.d.	n.d.
Titanite	n.d.	7.7	n.d.	n.d.	n.d.	41.7	n.d.	n.d.	17.9	n.d.
Ilmenite	n.d.	n.d.	n.d.	n.d.	1.9	n.d.	n.d.	29.6	n.d.	n.d.
Magnesioferrite	4.3	n.d.	n.d.	n.d.	1.7	n.d.	n.d.	28.4	n.d.	n.d.
Hematite	4.0	n.d.	n.d.	n.d.	n.d.	n.d.	n.d.	n.d.	n.d.	n.d.
Goethite	n.d.	n.d.	1.9	16.7	n.d.	n.d.	n.d.	n.d.	n.d.	n.d.
Barite	n.d.	n.d.	n.d.	n.d.	n.d.	n.d.	n.d.	n.d.	82.1	n.d.
Total	100.0	100.0	100.0	100.0	100.0	100.0	100.0	100.0	100.0	100.0

n.d. not detected.

Geology; Aristotle University of Thessaloniki.

2.3. Gamma-ray spectroscopy

The samples after oven-dried at 60 °C to constant weight, were measured using two high-resolution gamma ray spectrometry systems. The first one consisted of an HPGe coaxial detector with 42% efficiency and 2.0 keV resolution for 1.33 MeV photons shielded by 4″ Pb 1 mm Cd and 1 mm Cu and the second one consisted of a LEGe planar detector with 0.7 keV resolution for 122 keV photons, shielded by 3.3" Fe-Pb, 1 mm Cd and 1 mm Cu. The first spectrometry system with the High Purity Ge detector was used to measure the majority of the natural radionuclides examined in this study, except ^{238}U. The second one with the Low Energy planar Ge detector was used so as to determine only the concentration of ^{238}U, considering the low energy γ-ray of 63 keV emitted by its daughter ^{234}Th.

^{228}Ra concentration was measured as ^{228}Ac, using 911, 968 and 338 keV γ-rays and ^{228}Th concentration (measured as decay products in equilibrium, i.e. ^{212}Pb, using 238 and 300 keV γ-rays, ^{212}Bi, using 727 keV γ-ray and ^{208}Tl, using 2614, 583 and 860 keV γ-rays). The determination of ^{226}Ra content was based on measurement of ^{222}Rn decay product being in equilibrium. The measurement of ^{226}Ra from its own γ-ray at 186.25 keV introduces some problems because of the adjacent photo peak of ^{235}U at 185.75 keV, so that the isotopic ratio between ^{235}U and ^{238}U was considered being the natural one, i.e. 0.0072 and secular equilibrium between ^{238}U and ^{226}Ra had to be assumed.

Table 6
Weathering indices of the samples as described in Table 1.

	R	WIP	PWI	V	CIA	CIW	PIA
SN1	12.52	2901.87	91.25	1.90	51.67	62.15	52.52
SN2A	3.42	2122.79	5.38	2.30	72.22	75.36	74.24
SN3	5.84	2744.54	3.58	0.73	48.23	50.13	48.09
SN6	5.78	4577.30	3.40	1.41	48.72	55.73	48.29
SER1	6.12	3959.05	66.69	0.62	35.67	37.51	34.12
SER2	6.22	3750.67	64.17	0.81	40.63	43.64	39.13
SER3	5.21	3733.68	66.02	0.64	36.88	38.18	35.92
SER6	11.18	2937.43	88.61	3.05	58.83	71.37	63.61
SER7	8.83	4049.56	88.49	2.68	55.47	67.98	58.65
SER8	6.14	4869.97	74.56	0.92	38.69	43.18	35.72
SER11	6.05	4869.87	83.86	2.63	57.13	68.56	60.69
KP1	7.70	4912.29	87.18	1.32	44.44	52.63	41.93
LT1	7.09	3514.44	83.26	1.28	55.82	61.16	57.05
MYK3	5.66	5375.17	83.16	2.41	54.52	65.86	56.89
MYK4	5.45	5116.51	82.89	2.19	54.80	64.65	56.90
MYK5	5.36	4648.70	82.10	1.56	51.46	57.45	51.84
MYK2	6.35	4971.62	84.98	2.71	55.69	68.26	59.01
MYK17	6.92	4678.19	82.51	3.86	57.53	75.33	64.28
MYK15	8.38	4873.11	88.19	4.57	55.57	76.53	62.32
MYK11	5.08	5992.95	81.90	2.95	56.23	69.83	60.21
MYK13	9.35	4212.13	87.47	3.31	53.77	71.75	57.55
MYK14	5.13	2072.73	0.30	0.95	42.49	46.70	40.84
ARI1	11.24	3816.16	91.14	6.13	57.96	81.49	68.84
TRI1	10.51	3722.48	90.32	4.76	58.98	77.99	67.52
GI1	14.55	3256.32	92.93	7.39	56.86	83.47	68.93
NI1	7.94	4397.94	87.37	4.15	59.18	77.10	67.15
KRI1	8.84	4196.67	88.74	5.36	60.17	80.67	70.68
XYI1	10.95	2743.97	89.64	2.18	58.24	67.15	61.21

Accuracy in the measurements of ^{226}Ra concentrations by ^{222}Rn decay product depended on the integral trapping of radon gas in the sample volume. So, a small addition (~2%) of charcoal in powder form (less than 400 μm in size) was mixed with the sample before sealing it hermetically and storing it in a freezer during ^{222}Rn in-growth period (Manolopoulou et al., 2002).

The calibration of the gamma spectrometry systems was performed with the radionuclide specific efficiency method in order to avoid any uncertainty in gamma ray intensities as well as the influence of coincidence summation and self-absorption effects of the emitting gamma photons. A set of high-quality certified reference materials (RGU-1, RGTh-1, RGK-1) (IAEA, 1987) was used, with densities similar to the average beach sands measured after pulverization. Cylindrical geometry (volume of beakers = 50 cm^3) was used assuming that the radioactivity is homogenously distributed in the measuring samples. The samples were measured up to 2.3 days in order to achieve a Minimum Detectable Activity of 4 Bq kg^{-1} for ^{228}Ra, 2 Bq kg^{-1} for ^{228}Th, 2 Bq kg^{-1} for ^{226}Ra and 21 Bq kg^{-1} for ^{238}U, with 33% uncertainty. The total uncertainty of the radioactivity levels was calculated by propagation of the systematic and random errors of measurements. The systematic errors in the efficiency calibration ranges from 0.3 to 2% and the random errors of the radioactivity measurements extend up to 19% except in the ^{238}U measurement, where the error extends up to 50% for activities measured lower than 10 Bq kg^{-1}.

2.4. Determination of major, trace element contents

The major elements of the 28 sand samples were determined by ICP-MS, at Activation Laboratories (ACTLABS, Ontario, Canada) following a lithium borate fusion and dilute acid digestion. Fused sample was diluted and analysed by Perkin Elmer Sciex ELAN 9000 ICP/MS. Three blanks and five controls (three before sample group and two after) were analysed.

2.5. Powder X-ray diffractometry

Ten heavy concentrates of the sand samples were sent for mineral identification and semi-quantitative analysis at ACTLABS, Ontario, Canada.

A portion of each pulverized sample was loaded into a standard holder. The quantities of the crystalline mineral phases were determined using the Rietveld method which is based on the calculation of the full diffraction pattern from crystal structure information. The X-ray diffraction analysis was performed on a Panalytical X'Pert Pro diffractometer, equipped with a Cu X-ray source and an X'Celerator detector operating at the following conditions. 40 kV and 40 mA; range 5–70 deg 2θ; step size 0.017 deg 2θ; time per step 50.165 s; fixed divergence slit angle 0.5°; sample rotation 1 rev/sec.

2.6. Binocular microscope and SEM–EDS examination

In order to identify textural features of the sand grains and content of ferromagnesian minerals, all the samples were examined under the binocular microscope.

Since semi-quantitative P-XRD analyses were made, only major mineral constituents were determined. Therefore, five polished sections of the most enriched in heavy minerals (Fig. 3) were prepared including the grains of all samples and then were analysed by using a SEM-EDS JEOL JSM840A-INCA 300 at the Scanning Microscope Laboratory, Aristotle University of Thessaloniki in order to determine mineral phases and make comparisons between the beach sands and the adjacent granitoids. Eight sections from the granitoids of the Atticocycladic zone were also studied. Operating conditions were: accelerating voltage 20 kV, probe current 45 nA and counting time 60 s.

3. Results

The specific activities of ^{238}U, ^{226}Ra, ^{228}Ra and ^{228}Th (Bq/kg), along with the ^{226}Ra/^{238}U and ^{228}Th/^{228}Ra ratios and the respective standard errors and absolute differences are presented in Table 3. The absolute values of the differences between the ratios and 1 as a measure of the disequilibrium in both the U and Th- series radionuclides are also given.

Table 7
Pearson Correlation coefficients of the samples.

		[1-^{226}Ra/^{238}U]	R	WIP	PWI	V	CIA	CIW	PIA
[1-^{226}Ra/^{238}U]	Pearson Correlation	1	0.185	0.411[a]	0.491[b]	0.245	0.360	0.348	0.359
	Sig. (2-tailed)		0.347	0.030	0.008	0.209	0.060	0.070	0.061
	N	27	27	27	27	27	27	27	27
[1-^{228}Ra/^{228}Th]	Pearson Correlation	0.092	0.066	−0.183	0.017	−0.105	0.003	−0.052	−0.031
	Sig. (2-tailed)	0.643	0.738	0.352	0.930	0.594	0.987	0.792	0.875
	N	27	27	27	27	27	27	27	27

[a] Correlation is significant at the 0.05 level (2-tailed).
[b] Correlation is significant at the 0.01 level (2-tailed).

Table 8
Kendall's and Spearman's Correlation coefficients of the samples.

			[1-^{226}Ra/^{238}U]	R	WIP	PWI	V	CIA	CIW	PIA
Kendall's	[1-^{226}Ra/^{238}U]	Cor. Coef.	1.000	0.051	0.201	0.185	0.222	0.265	0.254	0.244
		Sig. 2-tailed	.	0.707	0.138	0.172	0.100	0.050	0.060	0.072
		N	27	27	27	27	27	27	27	27
	[1-^{228}Ra/^{228}Th]	Cor. Coef.	0.162	0.033	−0.149	−0.011	−0.050	−0.088	−0.044	−0.055
		Sig. 2-tailed	0.246	0.810	0.281	0.936	0.719	0.523	0.749	0.689
		N	27	27	27	27	27	27	27	27
Spearman's	[1-^{226}Ra/^{238}U]	Cor. Coef.	1.000	0.065	0.263	0.259	0.332	0.414[a]	0.368	0.383[a]
		Sig. 2-tailed	.	0.742	0.176	0.183	0.084	0.028	0.054	0.044
		N	27	27	27	27	27	27	27	27
	[1-^{228}Ra/^{228}Th]	Cor. Coef.	0.208	0.087	−0.237	0.036	−0.088	−0.138	−0.060	−0.083
		Sig. 2-tailed	0.288	0.661	0.224	0.857	0.656	0.482	0.762	0.675
		N	27	27	27	27	27	27	27	27

**Correlation is significant at the 0.01 level (2-tailed).
[a] Correlation is significant at the 0.05 level (2-tailed).

Table 9
Pearson Correlation coefficients of the heavy mineral enriched samples.

		[1-^{226}Ra/^{238}U]	R	WIP	PWI	V	CIA	CIW	PIA
[1-^{226}Ra/^{238}U]	Pearson Correlation	1	0.184	0.508	0.367	0.280	0.386	0.373	0.411
	Sig. (2-tailed)		0.692	0.244	0.418	0.543	0.393	0.410	0.360
	N	6	6	6	6	6	6	6	6
[1-^{228}Ra/^{228}Th]	Pearson Correlation	0.215	0.529	0.002	0.515	0.090	0.263	0.300	0.287
	Sig. (2-tailed)	0.643	0.223	0.996	0.237	0.848	0.569	0.513	0.533
	N	6	6	6	6	6	6	6	6

**Correlation is significant at the 0.01 level (2-tailed).

Table 10
Kendall's and Spearman's Correlation coefficients of the heavy minerals enriched samples.

			[1-^{226}Ra/^{238}U]	R	WIP	PWI	V	CIA	CIW	PIA
Kendall's	[1-^{226}Ra/^{238}U]	Cor. Coef.	1	0.195	0.098	0.293	0.390	0.683[a]	0.683[a]	0.683[a]
		Sig. 2-tailed	.	0.543	0.761	0.3620	0.224	0.033	0.033	0.033
		N	6	6	6	6	6	6	6	6
	[1-^{228}Ra/^{228}Th]	Cor. Coef.	0.150	0.000	−0.488	0.000	0.098	0.195	0.195	0.195
		Sig. 2-tailed	0.645	1.000	0.129	1.000	0.761	0.543	0.543	0.543
		N	6	6	6	6	6	6	6	6
Spearman's	[1-^{226}Ra/^{238}U]	Cor. Coef.	1.000	0.270	0.126	0.414	0.613	0.847[a]	0.847[a]	0.847[a]
		Sig. 2-tailed	.	0.558	0.788	0.355	0.144	0.016	0.016	0.016
		N	6	6	6	6	6	6	6	6
	[1-^{228}Ra/^{228}Th]	Cor. Coef.	0.191	0.072	−0.667	0.072	0.000	0.288	0.288	0.288
		Sig. 2-tailed	0.682	0.878	0.102	0.878	1.000	0.531	0.531	0.531
		N	6	6	6	6	6	6	6	6

**Correlation is significant at the 0.01 level (2-tailed).
[a] Correlation is significant at the 0.05 level (2-tailed).

Major element analyses used for the calculation of the weathering indices are given Table 4.

The semi-quantitative results of only the heavy fractions (heavy magnetic, HM and heavy non-magnetic HNM) have been ponderated to 100% and are given in Table 5.

The values of the weathering indices used in this study are given in Table 6.

The correlations between the radioactive secular equilibrium in ^{238}U and ^{232}Th- series have been assessed with Pearson's, Spearman's and Kendall's correlation coefficients. Pearson's correlation measures the strength of association between two variables. Spearman's correlation is a non-parametric test that is used to measure the degree of association between two variables and Kendall's correlation is a non-parametric test that measures the strength of dependence between two variables.

Pearson's correlation coefficients between the absolute differences from 1 of the radionuclide ratios and the weathering indices are given in Table 7 for all the samples and only for heavy minerals enriched samples in Table 9. In Tables 8 and 10, the correlation coefficients are given for Spearman's and Kendall's correlations for all the samples and only heavy minerals enriched samples respectively. Here it has to be noted that as sample MYK14 contains exceptionally high amounts of barite, Ra value is anomalously impacted by this mineral. Therefore, it would be not be considered in the correlation analyses, but its content will be shown in the rest of the Tables.

Samples with ^{226}Ra/^{238}U ratios close to 1 should be in radioactive secular equilibrium in time comparable to the half-lives of ^{234}U and ^{230}Th, which are the intermediate radionuclides between ^{238}U and ^{226}Ra in the ^{238}U radioactive series.

Most of the samples mostly contain quartz and feldspars, explaining the high SiO_2 plus Al_2O_3 values. These samples are typical beach sands. However, these samples would not tell a lot as far as their weathering and thus isotopic history are concerned, since their predominant mineral, quartz, is not susceptible to weathering. However, this is not the case for heavy-minerals enriched samples. The latter do not exhibit a uniform content of minerals. It seems to be high dependent from the type of the major (granite) or some minor parental rocks (metamorphics). Therefore, the key heavy mineral could vary from garnet,

allanite, epidote etc. (see Table 5).

The majority of granitic rocks of Atticocycladic zone are in $^{226}Ra/^{238}U$ and $^{228}Th/^{228}Ra$ secular equilibrium (Papadopoulos et al., 2013). Considering that the age of all the granitic rocks which are in most cases the most probable parental rocks of the beach sands studied is much higher than 1 Ma, secondary processes (rock–water interactions) in the last million of years most likely explain the significant shift to 1 in the $^{226}Ra/^{238}U$ ratios of some samples. This period is sufficient for the radionuclides to be separated and the radioactive disequilibrium to be preserved. However, samples exhibiting $^{226}Ra/^{238}U$ close to 1 are considered really unaltered during the above-mentioned periods (Gascoyne and Miller, 2001).

4. Discussion

As a result of radioactive secular disequilibrium, U has either leached, or Ra has been enriched in the respective systems. In general, U is geochemically more mobile than Ra in oxidizing environments as U^{+4} is oxidized to U^{+6}. On the other hand, Ra is more mobile than U in the presence of SO_4 and Cl anions, implying increased Ra solubility at saline waters (Herczeg et al., 1988). It has been observed that Ra adsorbed to river particles is desorbed under conditions of higher salinity as rivers empty into the ocean forming complexes with the available anions (chloride or associated sulphate and carbonate anions) as well as ion-exchange mechanisms (e.g. Li et al., 1977; Li and Chan, 1979; Gascoyne, 1992; Gascoyne and Schwarcz, 1986. Gascoyne and Miller, 2001; Dosseto et al., 2006, 2008; Plater et al., 1994; Mathieu et al., 1995; Vigier et al., 2001, 2005; 2006; Dequincey et al., 2002; Chabaux et al., 2003, 2006; 2008; Maher et al., 2004; De Paolo et al., 2006; Granet et al., 2007; Gaillardet, 2008; Pelt et al., 2008; Bourdon et al., 2009). In general, the radioactive disequilibrium between ^{226}Ra and ^{238}U indicates the selective deposition of ^{230}Th or ^{226}Ra, which are less soluble in water than U, depending on the pH-Eh conditions and ligand concentration in the interacting fluids (Ibrahiem, 2003).

As long as the distortion of the secular equilibrium in the above samples is quite recent in geological time, the reasons of the disequilibrium should be found at the low temperature geochemistry of U and Ra. Intensive leaching and transportation of U as U^{+6} at low temperatures can occur in the presence of various anions such as F^-, Cl^-, CO_3^{2-}, SO_4^{2-} and PO_4^{3-}. Consequently, U is generally more soluble in oxidising alkaline and carbonate-rich waters than in aciding reducing ones. Therefore, such conditions could be the reason of secular disequilibrium in the samples exhibiting $^{226}Ra/^{238}U > 1$. Assuming that the rock-water interaction history of the relatively young geologically samples is quite simple and remained unchanged, the presence of alkaline pH conditions and the absence of all the above anions except of PO_4^{3-}, are the geochemical conditions that favour the $^{226}Ra/^{238}U < 1$ values.

Radioactive disequilibria of ^{232}Th series in geochemical systems does not reveal so much information, since the time to reach radioactive secular equilibrium is very short (about 40 a which is six times the half-life of ^{228}Th). As the half-lives of ^{228}Ra and ^{228}Th are exceptionally short (5.75a and 1.91a respectively), the $^{228}Th/^{228}Ra$ ratios are less sensitive chemical weathering indicators compared to the $^{226}Ra/^{238}U$ ratios. This is shown in Table 3 where the $^{228}Th/^{228}Ra$ ratios are $1 \pm 1\sigma$ at almost all cases.

As seen from Table 3, the majority of the sand samples are close to radioactive secular equilibrium. Exception to that is sample MYK14 from Mykonos island. This sample is the most enriched in natural radionuclides, especially ^{228}Th, ^{228}Ra and ^{226}Ra. Compared to these radionuclides, ^{238}U is depleted. As discussed above, rock-water interactions should be responsible for this depletion. More specifically, extensive hydrothermal activity in the NW of Mykonos from where the sample MYK14 was taken is also proved from the abundance of barite in this particular sample. This SO_4^{-2} abundance has increased the solubility of Ra especially in saline waters (Herczeg et al., 1988). The enrichment in Ra other than U depletion is the most probable reason for the radioactive disequilibrium in this sample.

In Tables 6 and 7 the measure of U- and Th-series disequilibrium (as expressed by the absolute difference of both $^{226}Ra/^{238}U$ and $^{228}Th/^{228}Ra$ ratios from 1) are correlated with the values of the weathering indices for all the beach sand samples for the samples from Atticocycladic zone, using Pearson's, Spearman's and Kendall's correlation coefficients.

Statistically significant correlations are only present between ^{238}U-series disequilibrium and weathering indices. More specifically, WIP and especially PWI give statistically significant Pearson's correlations implying linear connection. Also, significant Spearman's correlations exist with CIA and PIA.

As explained above, the correlations between Th-series disequilibrium and the weathering indices are statistically insignificant in all cases. This confirms that Th-series disequilibrium is much less sensitive than U-series disequilibrium.

Considering that common beach sands are mainly consisted of quartz which is resistant to chemical weathering, more realistic results would arise if we only used heavy minerals enriched samples for correlations. These samples contain traces of quartz and feldspars and are mainly consisted of garnet, epidote, titanite, Fe-minerals (hematite, goethite magnesioferrite), allanite and Al-minerals (kyanite, sillimanite).

In Tables 8 and 9, the respective Pearson's, Kendall's and Spearman's correlation coefficients for only the heavy minerals are given.

Although no statistically significant results arise for Pearson's correlations, implying that there are no linear connections, Kendall's and Spearman's correlations are enhanced. There are statistically significant correlation coefficients between ^{238}U series disequilibrium and CIA, CIW and PIA which are quite strong especially in the case of Spearman's correlations.

These particular weathering indices are well correlated in the heavy minerals-enriched samples obviously because of the presence of feldspars that are altered to clay minerals, as well as the alteration of other minerals to clays such as garnets (to chlorite) or relative difference in mobility between Ca and alkalis.

5. Conclusions

The results are compared to weathering indices and suggest a significant linear correlation of U-series disequilibrium with WIP (alkaline and alkaline-earth element leaching) and PWI (silica leaching) for the beach sands studied and significant non-linear correlations with CIA (chemical index of alteration) and PIA (plagioclase index of alteration). Considering only the heavy mineral enriched samples, significant correlations exist between U-series disequilibrium and CIA, CIW (chemical index of weathering) and PIA.

This study shows that the use of U-series data can support and strenghten the interpretation of chemical weathering in sands provided by traditional weathering indexes.

The mineralogical composition affects the extent of weathering. By eliminating the presence of more stable and unaffected to weathering minerals (e.g. quartz) and considering only heavy mineral fractions that contain Fe-Mg minerals being susceptible to weathering, the correlation coefficients among especially CIA, PIA and U-series disequilibrium in beach sands show a remarkable increase, probably due to the high amounts of feldspars in the beach sands studied.

The use of Th-series disequilibrium as a weathering index is limited, due to ^{228}Th and ^{228}Ra geochemistry and especially due to their small radionuclide half-lives.

U-series disequilibrium can therefore be used as a relatively sensitive weathering index in sediments consistent with CIA. CIW and PIA indices. However, the mineralogical composition must be considered. The presence of susceptible to weathering minerals is a perquisite. More specifically, the mineral content of the sediments should involve

considerable amounts of sensitive to weathering minerals (e.g. Fe-Mg minerals) as well as feldspars.

Acknowledgments

This research has been funded by the IKY (Greek State Scholarships Foundation) fellowships of excellence for postgraduate studies in Greece –SIEMENS program.

The author would like to thank two anonymous reviewers for their constuctive comments that significantly improved the quality of the manuscript.

References

Altherr, R., Siebel, W., 2002. I-type plutonism in a continental back arc setting, Miocene granitoids and monzonites from the central Aegean Sea, Greece. Contrib. Mineral. Petrol. 143, 397–415.

Altherr, R., Kreuzer, H., Wendt, I., Lenz, H., Wagner, G.A., Keller, J., Harre, W., Hohndorf, A., 1982. A late Oligocene/early Miocene high temperature belt in the Attic–Cycladic crystalline complex (SE Pelagonian, Greece). Geol. Jahrb. E23, 97–164.

Altherr, R., Henjes-Kunst, F.J., Matthews, A., Friedrichsen, H., Hansen, B.T., 1988. O–Sr isotopic variations in Miocene granitoids from the Aegean, evidence for an origin by combined assimilation and fractional crystallisation. Contrib. Mineral. Petrol. 100, 528–541.

Bonotto, D.M., Andrews, J.N., Darbyshire, D.P.F., 2001. A laboratory study of the transfer of 234U and 238U during water–rock interactions in the Carnmenellis granite (Cornwall, England) and implications for the interpretation of field data. Appl. Radiat. Isot. 54, 977–994.

Bourdon, B., Bureau, S., Andersen, M.B., Pili, E., Hubert, A., 2009. Weathering rates from top to bottom in a carbonate environment. Chem. Geol. 258, 275–287.

Buick, I.S., 1991. The late Alpine evolution of an extensional shear zone, Naxos, Greece. J. Geol. Soc. Lond. 148, 93–103.

Chabaux, F., Bourdon, B., Riotte, J., 2008. U-series geochemistry in weathering profiles, river waters and lakes. Radioact. Environ. 13, 49–104.

Chabaux, F., Riotte, J., Dequincey, O., 2003. U-Th-Ra fractionation during weathering and river transport. Rev. Mineral. Geochem. 52, 533–576.

Chabaux, F., Granet, M., Pelt, E., France-Lanord, C., Galy, V., 2006. ^{238}U-^{234}U-^{230}Th disequilibria and timescale of sedimentary transfers in rivers: clues from the Gangetic plain rivers. J. Geochem. Explor. 88, 373–375.

Chapman, N.A., Smellie, J.A.T., 1986. Introduction and summary of the workshop: natural analogues to the conditions around a final repository for highlevel radioactive waste. Chem. Geol. 55, 167–173.

Condomines, M., Hermond, C., Allegre, C.J., 1988. U–Th–Ra radioactive disequilibria and magmatic processes. Earth Planet Sci. Lett. 90, 243–262.

De Paolo, D.J., Maher, K., Christensen, J.N., McManus, J., 2006. Sediment transport time measured with U-series isotopes: results from ODP North Atlantic drift site 984. Earth Planet Sci. Lett. 248, 394–410.

Dequincey, O., Chabaux, F., Clauer, N., Sigmarsson, O., Liewig, N., Leprun, J.-C., 2002. Chemical mobilizations in laterites: evidence from trace elements and ^{238}U-^{234}U-^{230}Th disequilibria. Geochem. Cosmochim. Acta 66, 1197–1210.

Dosseto, A., Bourdon, B., Gaillardet, J., Allegre, C.J., Maurice-Bourgoin, L., 2006. Weathering and transport of sediments in the Bolivian Andes: time constraints from uranium-series isotopes. Earth Planet Sci. Lett. 248, 759–771.

Dosseto, A., Bourdon, B., Turner, S.P., 2008. Uranium-series isotopes in river materials: insights into the timescales of erosion and sediment transport. Earth Planet Sci. Lett. 265 (1–2), 1–17.

Durr, S., Keller, J., Okrusch, M., Seidel, E., 1978. The median Aegean crystalline belt: stratigraphy, structure, metamorphism, magmatism. In: Closs, H., Roeder, D.H., Schmidt, K. (Eds.), Alps, Appenines, Hellenides, pp. 455–477.

Fedo, C.M., Nesbitt, H.W., Young, G.M., 1995. Unraveling the effects of potassium metasomatism in sedimentary rocks and paleosols, with implications for paleoweathering conditions and provenance. Geology 23, 921–924.

Gaillardet, J., 2008. Isotope geochemistry as a tool for deciphering kinetics of water-rock interaction. In: Brantley, S.L., Kubicki, J.D., White, A.F. (Eds.), Kinetics of Water-rock Interaction. Springer, New York, pp. 591–653.

Gascoyne, M., 1992. The geochemistry of the actinides and their daughters. In: Ivanovich, M., Harmon, R.S. (Eds.), Uranium-series Disequilibrium: Applications to Earth, Marine, and Environmental Sciences, second ed. Clarendon Press, Oxford, pp. 3458.

Gascoyne, M., Miller, N.H., 2001. Uranium-series disequilibrium in tuff and granite: hydrogeological Implications. In: Proceedings of the 9th International High-level Radioactive Waste Management Conference. American Nuclear Society, La Grange Park, IL CD-ROM file 06-4.pdf.

Gascoyne, M., Schwarcz, H.P., 1986. Radionuclide migration over recent geologic time in a granitic pluton. Chem. Geol. 59, 75–85.

Gascoyne, M., Cramer, J.J., 1987. History of actinide and minor element mobility in an Archean granitic batholith in Manitoba. Appl. Geochem. 2, 37–53.

Granet, M., Chabaux, F., Stille, P., France-Lanord, C., Pelt, E., 2007. Time-scales of sedimentary transfer and weathering processes from U-series nuclides: clues from the Himalayan rivers. Earth Planet Sci. Lett. 261, 389–406.

Guthrie, V., 1991. Determination of recent ^{238}U, ^{234}U and ^{230}Th mobility in granitic rocks: application of a natural analogue to the high-level waste repository environment. Appl. Geochem. 6, 63–74.

Guttman, J., Kronfeld, J., 1982. Tracing interaquifer connections in the Kefar Uriyya-Agur region (Israel), using natural uranium isotopes. J. Hydrol. 55, 145–150.

Harnois, L., Moore, J.M., 1988. Geochemistry and origin of the ore chimney formation: a transported paleoregolith in the grenville province of southeastern Ontario, Canada. Chem. Geol. 69, 267–289.

Henjes-Kunst, F., Altherr, R., Kreuzer, H., Hansen, B.T., 1988. Disturbed U–Th–Pb systematics of young zircons and uranothorites, the case of the Miocene Aegean granitoids (Greece). Chem. Geol. 73, 125–145.

Herczeg, A.L., Simpson, H.J., Anderson, R.F., Trier, R.M., Mathieu, G.G., Deck, B.L., 1988. Uranium and radium mobility in groundwaters and brines within the Delaware basin, Southeastern New Mexico, U.S.A. Chem. Geol. 72, 181–196.

I.A.E.A, 1987. Preparation of Gamma-ray Spectroscopy Reference Materials RGU-1, RGTh-1 and RGK-1 Report- IAEA/RL/148. International Atomic Energy Agency, Vienna 1987.

Ibrahiem, N.M., 2003. Radioactive disequilibrium in the different rocktypes in wadi wizr, the eastern desert of Egypt. Appl. Radiat. Isot. 58, 385–392.

Iglseder, C., Grasemann, B., Schneider, D.A., Petrakakis, K., Miller, C., Klötzli, U.S., Thöni, M., Zámolyi, A., Rambousek, C., 2009. I and S-type plutonism on Serifos (W-Cyclades, Greece). Tectonophysics 473, 69–83.

Ivanovich, M., Harmon, R.S., 1982. Uranium Series Disequilibrium: Applications to Environmental Problems. Clarendon Press, Oxford.

Ivanovich, M., Harmon, R.S., 1992. Uranium-series Disequilibrium: Applications to Earth, Marine, and Environmental Sciences, second ed. Clarendon Press, Oxford.

Latham, A.G., Schwarcz, H.P., 1987. The relative mobility of U, Th and Ra isotopes in the weathered zone of the Eye-Dashwa Lakes granite pluton, Northwestern Ontario, Canada. Geochem. Cosmochim. Acta 51, 2787–2793.

Li, Y.H., Chan, L.H., 1979. Desorption of Ba and ^{226}Ra from river-borne sediments in the Hudson estuary. Earth Planet Sci. Lett. 43, 343–350.

Li, Y.H., Mathieu, G.G., Biscaye, P., Simpson, H.J., 1977. The flux of ^{226}Ra from estuarine and continental shelf sediments. Earth Planet Sci. Lett. 37, 237–241.

Maher, K., De Paolo, D.J., Lin, J.C.F., 2004. Rates of silicate dissolution in deep-sea sediment: in situmeasurement using U-234/U-238 of pore fluids. Geochem. Cosmochim. Acta 68, 4629–4648.

Manolopoulou, M., Stoulos, S., Mironaki, D., Papastefanou, C., 2002. A new technique for accurate measurements of Ra-226 with γ-spectroscopy in voluminous samples. Nucl. Instrum. Methods A 508, 362–366.

Mastrakas, N., 2006. Tinos Pluton and Associated Skarn Formations. PhD thesis. University of Patras, pp. 227 (In Greek).

Mathieu, D., Bernat, M., Nahon, D., 1995. Short-lived U and Th isotope distribution in a tropical laterite derived from Granite (Pitinga river basin, Amazonia, Brazil): application to assessment of weathering rate. Earth Planet Sci. Lett. 136, 703–714.

Maynard, J.B., Sutton, S.J., Robb, L.J., 1995. A paleosol developed on hydrothermally altered granite from the hinterland of the Witwatersrand Basin: characteristics of a source of basin fill. J. Geol. 103, 357–377.

Menant, A., Jolivet, L., Augier, R., Skarpelis, N., 2013. The North Cycladic detachment system and associated mineralization, Mykonos, Greece, insights on the evolution of the Aegean domain. Tectonics 32, 1–20.

Nesbitt, H.W., Young, G.M., 1982. Early proterozoic climates and plate motions inferred from major element chemistry of lutites. Nature 299.

Nesbitt, H.W., Young, G.M., 1984. Prediction of some weathering trends of plutonic and volcanic rocks based on thermodynamic and kinetic considerations. Geochem. Cosmochim. Acta 48, 1523–1534.

Nesbitt, H.W., Young, G.M., 1989. Formation and diagenesis of weathering profiles. J. Geol. 97, 129–147.

Osmond, J.K., Cowart, J.B., 1976. The theory and uses of natural uranium isotopic variations in hydrology. At. Energy Rev. 14, 621–678.

Osmond, J.K., Cowart, J.B., 1982. Groundwater. In: Ivanovich, M., Harmon, R.S. (Eds.), Uranium Series Disequilibrium: Applications to Environmental Problems. Clarendon Press, Oxford, pp. 202–245.

Osmond, J.K., Cowart, J.B., Ivanovich, M., 1983. Uranium isotopic disequilibrium in ground water as an indicator of anomalies. Int. J. Appl. Radiat. Isot. 34, 283–308.

Papadopoulos, A., Christofides, G., Koroneos, A., Stoulos, S., Papatefanou, C., 2013. Radioactive secular equilibrium in ^{238}Uand ^{232}Th series in granitoids from Greece. Appl. Radiat. Isot. 75, 95–104.

Papadopoulos, A., Koroneos, A., Christofides, G., Papadopoulou, L., Tzifas, I., Stoulos, S., 2016a. Assessment of gamma radiation exposure of beach sands in highly touristic areas associated with plutonic rocks of the Atticocycladic zone (Greece). J. Environ. Radioact. 162, 235–243.

Papadopoulos, A., Koroneos, A., Christofides, G., Stoulos, S., 2016b. Comparison of ^{226}Ra/^{238}U and ^{228}Th/^{228}Ra disequilibrium with weathering indixes in beach sand sediments from Greece. J. Sediment. Res. 86, 668–682.

Papadopoulos, A., 2018. Geochemistry and REE content of beach sands along the Atticocycladic coastal zone, Greece. Geosci. J. 22 (6), 955–973.

Parker, A., 1970. An index of weathering for silicate rocks. Geol. Mag. 107, 501–504.

Pelt, E., Chabaux, F., Innocent, C., Navarre-Sitchler, A.K., Sak, P.B., Brantley, S.L., 2008. Uranium–thorium chronometry of weathering rinds: rock alteration rate and paleoisotopic record of weathering fluids. Earth Planet Sci. Lett. 276, 98–105.

Pe-Piper, G., 2000. Origin of S-type granites coeval with I-type granites in the Hellenic subduction system, Miocene of Naxos, Greece. Eur. J. Mineral 12, 859–875.

Pe-Piper, G., Piper, D.J.W., 2002. The Igneous Rocks of Greece, the Anatomy of an Orogen. Borntraeger, Berlin, pp. 573.

Pe-Piper, G., Kotopouli, C.N., Piper, D.J.W., 1997. Granitoid rocks of Naxos, Greece, regional geology and petrology. Geol. J. 32, 153–171.

Pe-Piper, G., Piper, D.J.W., Matarangas, D., 2002. Regional implications of geochemistry and style of emplacement of Miocene I-type diorite and granite, Delos, Cyclades,

Greece. Lithos 60, 47–66.
Plater, A.J., Dugdale, R.E., Ivanovich, M., 1994. Sediment yield determination using uranium-series radionuclides: the case of the Wash and Fenland drainage basin. Eastern England. Geomorphology 11, 41–56.
Rihs, S., Gontier, A., Turpault, M.-P., Lemarchand, D., Voinot, A., Chabaux, F., 2013. Insight into Biotite Weathering Rate Using U-series Isotopes [Abstract]: Goldschmidt2013, Conference Abstracts. pp. 2063.
Roaldset, E., 1972. Mineralogy and geochemistry of quaternary clays in the numedal area, southern Norway. Norsk. Geolisk. Tidsskrift. 52, 335–369 1972.
Rosholt, J.N., 1983. Isotopic composition of U and Th in crystalline rocks. J. Geophys. Res. 88, 7315–7330.
Ruxton, B.P., 1968. Measures of the degree of chemical weathering of rocks. J. Geol. 76, 518–527.
Schwarcz, H.P., Gascoyne, M., 1984. Uranium Series Dating of Quaternary Deposits, Quaternary Dating Methods. W.C. Mahaney, pp. 33–51.
Schwarcz, H.P., Gascoyne, M., Ford, D.C., 1982. Uranium series disequilibrium studies of granitic rocks. Chem. Geol. 36, 87–102.
Skarpelis, N., Tsikouras, B., Pe-Piper, G., 2008. The Miocene igneous rocks in the Basal Unit of Lavrion (SE Attica, Greece), petrology and geodynamic implications. Geol. Mag. 145, 1–15.
Smellie, J.A.T., 1982. Radioactive disequilibria in mineralized drill core samples from the Bjorklund uranium occurrence, Northern Sweden. SKBF (Svensk Klrnbdnsleforsorjning A.B.)/Klrnbransleslkerhet (KBS), Stockholm. Tech. Rep. 82–15, 26.
Smellie, J.A.Z., Mackenzie, A.B., Scott, R.D., 1986. An analogue validation study of natural radionuclide migration in crystalline rocks using uranium-series disequilibrium studies. Chem. Geol. 55, 233–254.
Souri, T., Watanabe, M., Sakagami, K., 2006. Contribution of parker and product indexes to evaluate weathering condition of yellow Brown forest soils in Japan. Geoderma 130, 346–355.
Stouraiti, C., Mitropoulos, P., Tarney, J., Barreiro, B., McGrath, A.M., Baltatzis, E., 2010. Geochemistry and petrogenesis of late Miocene granitoids, Cyclades, southern Aegean, Nature of source components. Lithos 114, 337–352.
Vigier, N., Bourdon, B., Turner, S., Allegre, C.J., 2001. Erosion timescales derived from U-decay series measurements in rivers. Earth Planet Sci. Lett. 193, 485–499.
Vigier, N., Bourdon, B., Turner, S., Van Calsteren, P., Subramanian, V., Dupre, B., Allegre, C.J., 2005. Parameters influencing the duration and rates of weathering deduced from U-series measured in rivers: the Deccan trap region (India). Chem. Geol. 219, 69–91.
Vigier, N., Burton, K.W., Gislason, S.R., Rogers, N.W., Duchene, S., Thomas, L., Hodge, E., Schaefer, B., 2006. The relationship between riverine U-series disequilibria and erosion rates in a basaltic terrain. Earth Planet Sci. Lett. 249, 258–273.